JOC The Journal of Organic Chemistry

pubs.acs.org/joc Article

Synthesis and Transport Studies of a Cofacial Porphyrin Cyclophane

Patrick Zwick,[¶] Chunwei Hsu,[¶] Maria El Abbassi, Olaf Fuhr, Dieter Fenske, Diana Dulić, Herre S. J. van der Zant,* and Marcel Mayor*

Cite This: J. Org. Chem. 2020, 85, 15072−15081 Read Online

ACCESS | Metrics & More | Article Recommendations | Supporting Information

ABSTRACT: Porphyrin cyclophane **1**, consisting of two rigidly fixed but still movable cofacial porphyrins and exposing acetate-masked thiols in opposed directions of the macrocycle, is designed, synthesized, and characterized. The functional cyclophane **1**, as pioneer of mechanosensitive 3D materials, forms stable single-molecule junctions in a mechanically controlled break-junction setup. Its reliable integration in a single-molecule junction is a fundamental prerequisite to explore the potential of these structures as mechanically triggered functional units and devices.

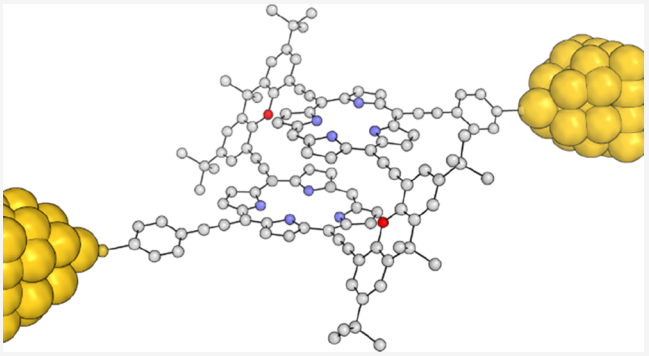

INTRODUCTION

Molecular-junction investigation, as the first step of fundamental structure−property relationship studies of single molecules integrated into electric circuits, is a crucial research field toward establishing possible future devices. The successful implementation of functional molecules into electronic circuits exposing functionalities such as rectification[1−3] or switching[4−10] by the application of an external stimulus that forces the molecules into one of two discrete conductance states has been reported. Resistance response upon conformational changes of a molecular junction by quantum interference while altering the electrode's distances was reported for oligophenylethynylenes (OPEs) in a mechanically controlled break-junction (MCBJ) and imidazole derivatives using the scanning-tunnelling microscopy break-junction technique.[11,12] In these cases, the spatial arrangement of a pair of stacking π-systems attached to opposed electrodes is manipulated with respect to each other in a bimolecular junction. Single-molecule mechano-manipulation in MCBJs was achieved resulting in alternating spin states by ligand field distortion and further indicated the compression and elongation of helically arranged π-systems.[13−15] As first model compounds, rigid rots comprising [2.2]para-cyclophanes (PCPs) have been integrated in molecular junctions to investigate their mechanosensitivity. Indeed, the resistance of the springlike single-molecule junction could be controlled by distance modulation mechanically, with oscillations as a function of the electrode distance of more than an order of magnitude in conductance. Quantum chemistry calculations indicated this phenomenon to arise from destructive quantum interference effects between the frontier orbitals of the modulated π-systems.[16]

Porphyrins are key components in nature's machinery to store energy via photosynthesis.[17] Their well-established synthesis as well as their rich and fine-tuneable electrical and optical properties make them particularly appealing building blocks for the construction of molecular devices.[18−20] Conductance features of porphyrin wires and tapes as well as different anchorings to the electrode's surface have been studied.[21−24] In our previous work, we showed that porphyrins form stable single-molecule junctions in a MCBJ setup in which three different conductance pathways were distinguished using an unsupervised clustering algorithm.[25] From a molecular design perspective, porphyrins have an additional appealing structural feature: They enable the perpendicular/right-angled arrangement of functional subunits in their meso positions. This makes them ideal building blocks to construct a cyclophane that allows mechanical manipulation of two cofacial porphyrins into the electrode direction by the compensation of the physical stress over laterally attached bridging units. Mechanical manipulation of such a cofacial $\pi-\pi$ structure because of a continuously adjustable stimulus is expected to yield a distinct conductance response, which possibly opens the door to a new class of mechano-sensitive molecular electronic components, such as potentiometers. Inspired by the topology of PCPs and our previous findings, we desired to design, synthesize, and investigate porphyrin cyclophanes, suitable for mechanosensi-

Received: August 12, 2020
Published: November 9, 2020

https://dx.doi.org/10.1021/acs.joc.0c01957
J. Org. Chem. 2020, 85, 15072−15081

tive single-molecule conductance experiments. Our first attempts toward mechanosensitive porphyrin cyclophanes were based on integrating a pair of porphyrin subunits into an OPE macrocycle. While our synthetic strategy did not yield the desired structure, yet the isolated threefold interlinked porphyrin dimer indicated the suitability of MCBJ experiments to study complex multilevel porphyrin architectures.[26]

In this work, we report the synthesis and characterization of zinc(II) porphyrin cyclophanes **1** with its structural isomer **2**, having the thioacetates in the same direction of the macrocycle. Additionally, we test the suitability of this new family of cyclophanes in MCBJ experiments with **1**.

RESULTS AND DISCUSSION

Design. The cofacial porphyrin cyclophane **1** is decorated with one acetal-masked thiol gold-anchoring group per porphyrin subunit, pointing into opposed directions of the macrocycle as shown in Figure 1. Planar xanthene units bridge

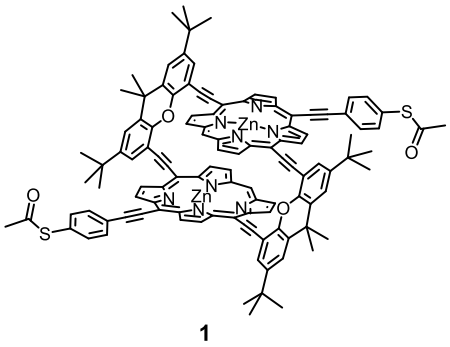

1

Figure 1. Chemical structure of the target compound **1**.

the macrocycle in the lateral positions of the porphyrins with respect to the anchoring groups. This ensures rigidity of the macrocyclic structure, while acetylenes between the bridge and the porphyrins provide revolving joints. The combination of rigid building blocks with revolving joints promises a controlled variation of the cofacial porphyrin arrangement upon mechanical manipulation of the electrode spacing.

When the structure is implemented into a molecular junction, distance modulation of the electrodes can be depicted as pulling and pushing on the anchoring groups of the macrocycle. Increasing and decreasing the distance of the electrodes should thus be compensated by a translational movement of the porphyrin planes with respect to each other. At the same time, the spacing between the two porphyrin planes should be altered. While detailed insights into the mechanisms of such conformational responses to the distance modulation will require in-depth analysis and theoretical studies, the working principle of the mechano-sensitive conformational response of the target structure **1** is outlined in Figure 2. As a guide for the eye, the distances of the two porphyrins between each other upon manipulating the electrode distance are visualized by arrows.

Retrosynthesis. The retrosynthetic plan toward **1** is displayed in Scheme 1. In a first step, the thioacetate functional groups were planned to be *trans*-protected from their *tert*-butyl analogues, which are suitably stable regarding the conditions required for the overall synthesis. The formation of the macrocyclic structure was expected to be accessible by a palladium-mediated fourfold Sonogashira−Hagihara cross-coupling reaction of two molecules of **3** and two molecules of 2,7-di-*tert*-butyl-4,5-diiodo-9,9-dimethyl-9*H*-xanthene[27] (**4**) under high dilution conditions. The highly functionalized porphyrin monomer **3** exposing both acetylenes for the macrocyclization after liberation of the tri-*iso*-propyl (TIPS)-protecting groups and a single thio-decorated phenyl acetylene was divided into single-brominated zinc complex **5** and *tert*-butyl-(4-ethynylphenyl)sulfane[28] by means of Sonogashira−Hagihara cross-coupling. Statistic bromination and metalation of 5,15-bis((tri-*iso*-propylsilyl)ethynyl)porphyrin[29] (**6**) should provide **5**.

Synthesis and Characterization. The synthetic overview is given in Scheme 2; detailed analytical data can be found in the Supporting Information.

In contrast to the *meso*-bromination of arylporphyrins by *N*-bromosuccinimide (NBS), the 10,20 *meso*-di-bromination of 5,15 *meso*-acetylene-decorated porphyrins are known to need a central magnesium(II) ion incorporated into the *tetra*-dentate ligand in order to increase the electron density in the *meso*-positions.[30] We found a suitable pseudo-one-pot, three-step procedure for the statistical monobromination of **6** yielding **7** in 44% while recovering 33% of **6** involving one single silica gel column during isolation.

Treatment of a solution of **6** in CH_2Cl_2 with di-*iso*-propylethylamine (N^iPr_2Et) and magnesium(II) iodide (MgI_2) at room temperature (rt) provided the magnesium complex of **6** quantitatively within an hour (h) as indicated by thin-layer chromatography (TLC) monitoring of the reaction. After aqueous workup, the crude product was subjected to bromination conditions using 1.1 equiv of NBS in a chloroform/pyridine solution. After 16 h of stirring at rt in the absence of light, the mixture was washed with water, and the separated organic phase was treated with trifluoroacetic acid (TFA) and stirred for 2 h at rt. After aqueous workup, the crude material was subjected to silica gel column chromatography (toluene 1:4 cyclohexane) where the desired monobrominated product **7** was isolated as the second eluting purple band besides the substrate **6** being the third eluting band. Treatment of a solution of **7** in CH_2Cl_2/CH_3OH with an excess of zinc(II) acetate [$Zn(OAc)_2$] afforded **5** quantitatively within 2 h at rt. Subsequent Sonogashira−Hagihara cross-coupling of **5** and *tert*-butyl-(4-

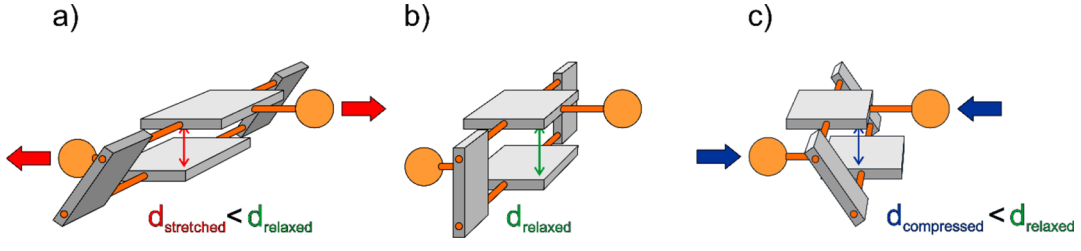

Figure 2. Proposed working principle of the laterally interlocked, mechano-sensitive porphyrin cyclophane **1**.

https://dx.doi.org/10.1021/acs.joc.0c01957
J. Org. Chem. 2020, 85, 15072−15081

Scheme 1. Retrosynthetic Analysis toward 1

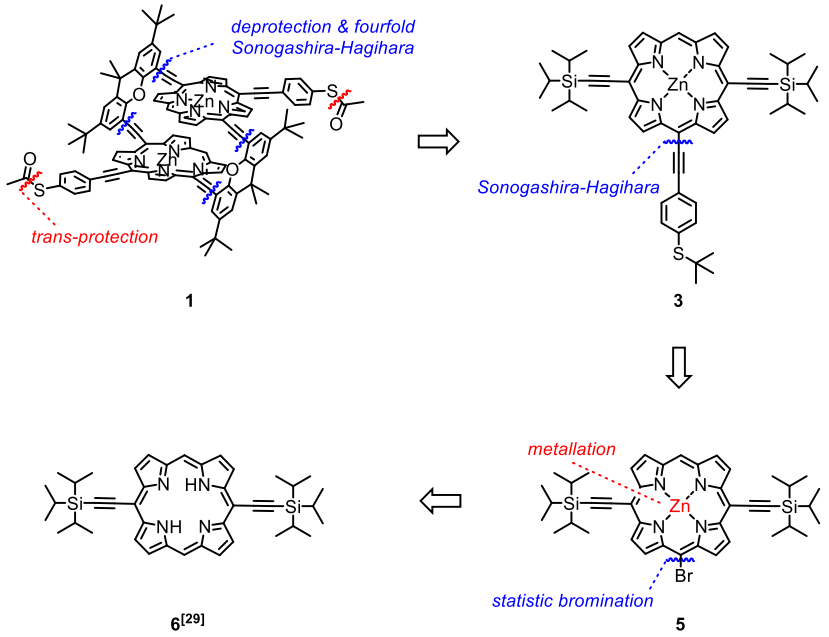

Scheme 2. Synthetic Overview; (a) MgI_2, CH_2Cl_2, N^iPr_2Et, rt, 1 h; (b) NBS, $CHCl_3$, C_5H_5N, rt, 16 h; (c) CF_3CO_2H, CH_2Cl_2, rt, 2 h; (d) $Zn(OAc)_2$, CH_2Cl_2, CH_3OH, rt, 2 h; (e) *tert*-butyl-(4-ethynylphenyl)sulfane, $Pd(PPh_3)_4$, CuI, THF, NEt_3, 50 °C, 16 h; (f) (1) TBAF, THF, rt, 1 h; (2) $Pd(PPh_3)_4$, CuI, THF, NEt_3, 80 °C (Sealed Tube), 16 h; (g) $Bi(OSO_2CF_3)_3$, AcCl, rt, 12 h; (h) $Zn(OAc)_2$, CH_2Cl_2, CH_3OH, rt, 1 d

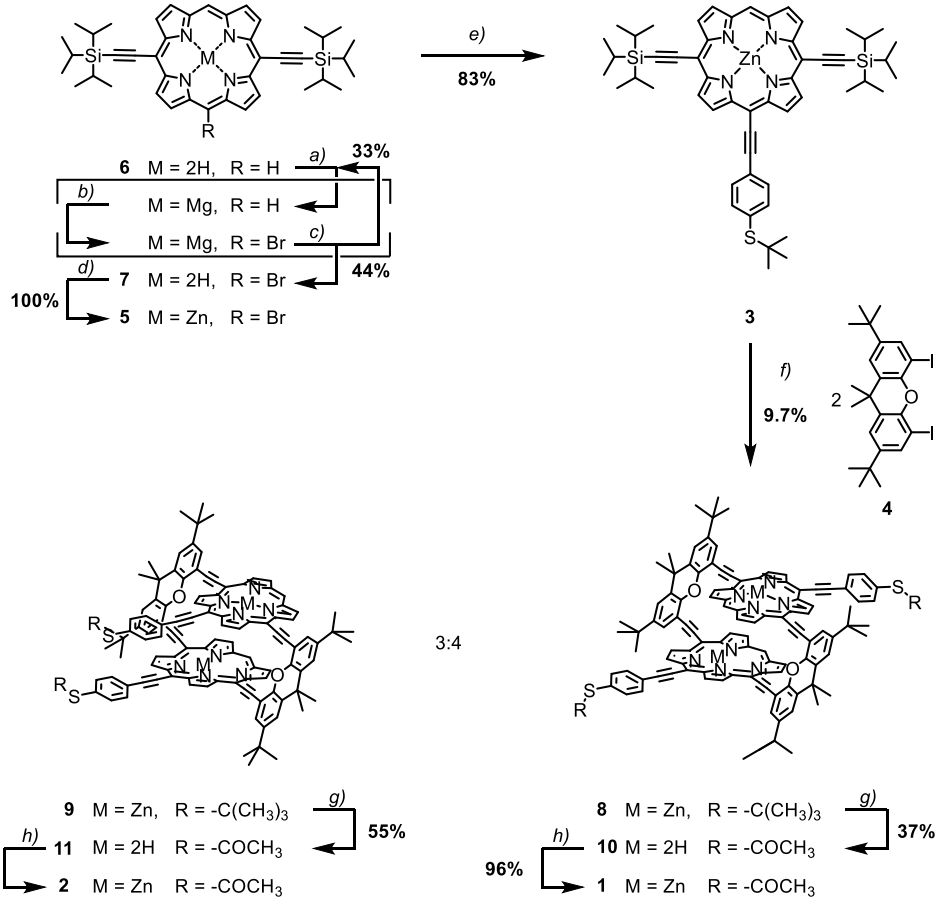

ethynylphenyl)sulfane at elevated temperatures of 50 °C mediated by palladium(0) tetrakis(triphenylphosphine) [$Pd(PPh_3)_4$] and copper(I) iodide (CuI) in degassed tetrahydrofuran (THF) and triethylamine (NEt_3) afforded analytically

https://dx.doi.org/10.1021/acs.joc.0c01957
J. Org. Chem. 2020, 85, 15072−15081

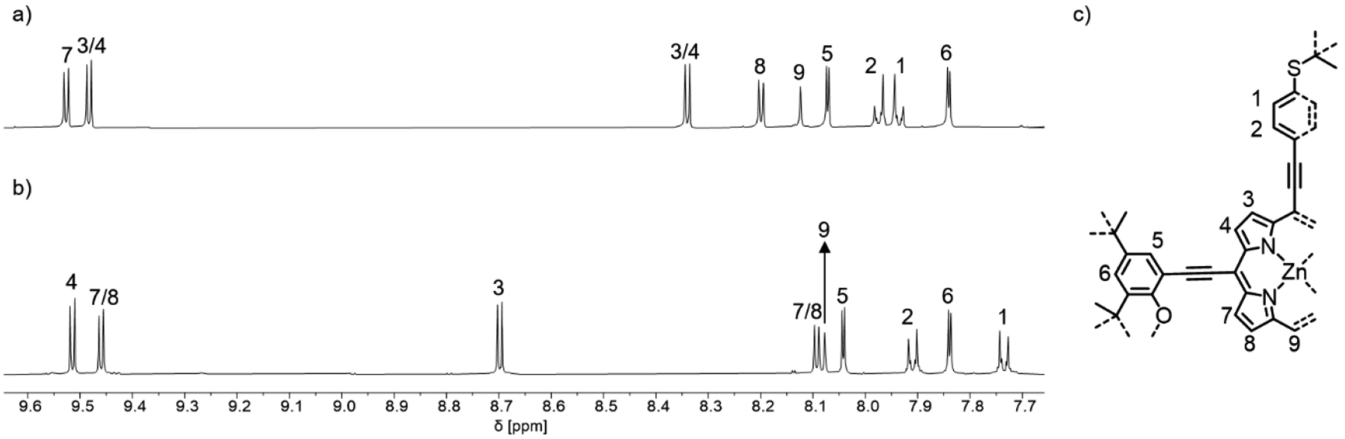

Figure 3. Stacked aromatic region of the ^{1}H NMR spectra of (a) **8** and (b) **9** recorded in THF-d_8 at 298 K operating on a 500 MHz proton frequency. (c) Symmetry-reduced and labelled structures of **8** and **9**.

pure **3** by reprecipitation of the crude reaction mixture from CH_2Cl_2/CH_3OH after filtration over a short silica plug eluted with CH_2Cl_2 in good yields of 83%.

A one-to-one mixture of **3** and **4** in wet THF, thoroughly degassed by purging with argon, was treated with excess tetra-*n*-butyl ammonium fluoride (TBAF) to liberate the TIPS-protected acetylenes of **3**. Once the reaction was completed as indicated by TLC, the mixture was cannula-transferred into a previously degassed solution of THF and NEt_3 containing $Pd(PPh_3)_4$ and CuI. The resulting 1 M solution of deprotected **3** and **4** was sealed under argon and placed in a preheated oil bath at 80 °C where it was vigorously stirred for 16 h. The mixture was evaporated to dryness, and the residue was subjected to silica gel column chromatography (CH_2Cl_2 1:1 cyclohexane). The eluted purple fraction comprising molecules with the expected masses of the target macrocycle as well as open-chain oligomers [determined by matrix-assisted laser-desorption ionization time-of-flight mass spectrometry (MALDI-ToF-MS)] was collected, concentrated, and subjected to automated recycling gel permeation chromatography (GPC) in chloroform. The slowest running and the second slowest running bands showing typical UV−vis traces for porphyrins were collected and evaporated to dryness. Both compounds were found to have the same mass by means of high-resolution electronspray-ionization time-of-flight mass spectrometry (HR-ESI-ToF-MS), fitting the molecular composition of macrocycles **8** and **9**. The observed difference in hydrodynamic radii while performing GPC led to the conclusion that the slowest eluting band should be the geminally interlocked porphyrin cyclophane **9**, while the band showing a slightly increased hydrodynamic radius was proposed to be target 5, pseudo 15-functionalized porphyrin cyclophane **8**. Macrocycles **8** and **9** were isolated in yields of 5.4 and 4.2%, respectively. The expected signals of the macrocyclic structures were observed in the proton nuclear magnetic resonance (^{1}H NMR) spectrum of the individual samples, with distinct differences in the chemical shifts of the signals but not in their number and multiplicities. Four low-field aromatic ^3J-doublets corresponding to the β-protons (3, 4, 7, and 8 in Figure 3), one single singlet for the meso-proton (9 in Figure 3), two aromatic ^4J-doublets of the xanthene bridge (5 and 6 in Figure 3), and an aromatic AB system arising from the anchoring group bearing phenyl (1 and 2 in Figure 3) were observed in the aromatic region, as assigned by two-dimensional ^{1}H−^{1}H nuclear Overhauser enhancement spectroscopy (Figures S25, S26, S34, and S35).

The UV−vis spectrum of the samples showed a symmetric Soret band, typical for rigidly bridged porphyrin cyclophanes.[31] The absence of exciton coupling between the two porphyrins indicated parallelism of the $\pi-\pi$ system in solution. The Soret bands of the macrocyclic structures **8** [λ_{Soret} = 442 nm, log(ε) = 5.56] and **9** [λ_{Soret} = 437 nm, log(ε) = 5.62] were found to be blue-shifted in comparison to the monomer **3** [λ_{Soret} = 447 nm, log(ε) = 5.61], while the Q bands of **8** [λ_{Q1} = 595 nm, log(ε) = 4.10 and λ_{Q2} = 645 nm, log(ε) = 4.52] and **9** [λ_{Q1} = 593 nm, log(ε) = 4.20 and λ_{Q2} = 642 nm, log(ε) = 4.58] appeared red-shifted compared to **3** [λ_{Q1} = 581 nm, log(ε) = 4.45 and λ_{Q2} = 627 nm, log(ε) = 4.31] as shown in Figure 4.

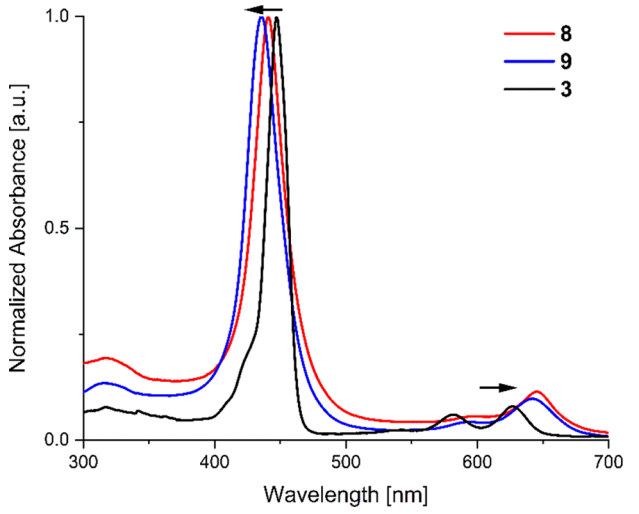

Figure 4. Normalized UV−vis spectra of **3** (black), **8** (red), and **9** (blue) recorded in CH_2Cl_2. Changes from monomer to cyclophane are visualized by black arrows.

Single crystals suitable for X-ray analysis were obtained by top-layering a THF solution of **8** and **9** with methanol (see Figure 5). Extracted from these solid-state structures, the porphyrin-to-porphyrin plane distance of **8** was determined to be 3.24 Å, thus 0.16 Å smaller than the carbon-to-carbon van der Waals distance. The thiol-to-thiol distance of the target 5, pseudo 15-functionalized porphyrin cyclophane **8**, was extracted

https://dx.doi.org/10.1021/acs.joc.0c01957
J. Org. Chem. 2020, 85, 15072−15081

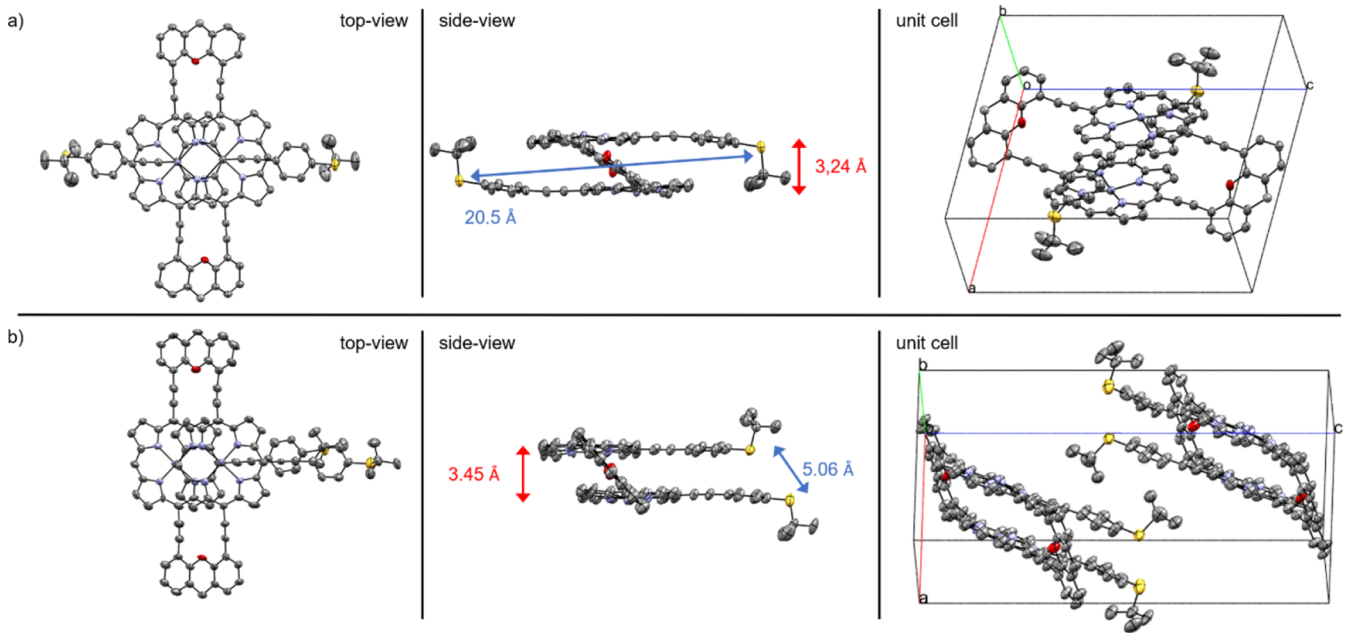

Figure 5. Oak Ridge thermal ellipsoid plot representation of the solid-state structure of (a) **8** and (b) **9**. Thermal ellipsoids are plotted on a 50% probability level. Solvent molecules, solubilizing groups, and hydrogen atoms are omitted for clarity. Red arrows indicate the plane-to-plane distances; blue arrows indicate the thiol-to-thiol distances.

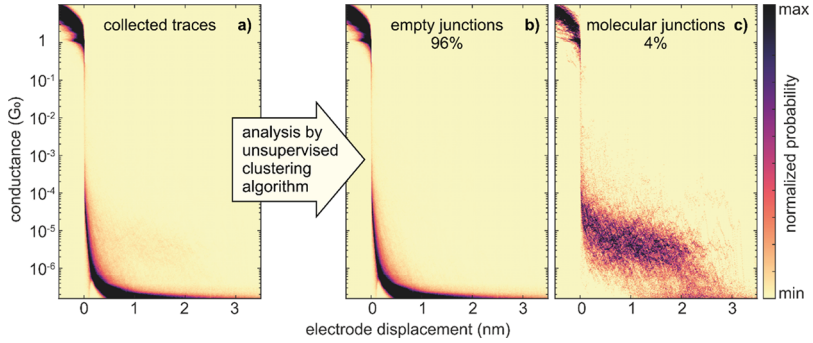

Figure 6. (a) Two-dimensional conductance-displacement histogram built from 5′113 consecutive breaking traces. The measurement is performed after the deposition of a 5 μM dichloromethane solution containing **1**. The applied bias is 100 mV, and the electrode speed is 2.5 nm/s. (b) Tunnelling and (c) molecular breaking traces separated from (a) by the clustering method shown in ref 36 with two classes. The yield of the molecular traces obtained from the clustering method is approximately 4%.

to be 20.5 Å. The geminally interlocked porphyrin cyclophane **9**, on the other hand, showed an increased plane-to-plane distance of 3.45 Å and a short thiol-to-thiol distance of 5.06 Å, compared to **8**, in the solid-state structure.

Both of these isomers (**8** and **9**) were subjected to *trans*-protection conditions in order to make the structures suitable to contact noble metal surfaces *via in situ* deprotection of the thioacetates upon formation of a covalent S−Au bond. **8** and **9** were each dissolved in dry and degassed toluene/acetonitrile and 175 equiv acetyl chloride (AcCl) in separate flasks under an argon atmosphere. The mixtures were treated with 3 equiv of bismuth(III) trifluoromethanesulphonate [$Bi(OSO_2CF_3)_3$] and stirred for 12 h at ambient temperature. TLC monitoring confirmed the completion of the reactions, and MALDI-ToF-MS analysis of the crude reaction mixtures revealed that besides *trans*-protection of the *tert*-butyl thioethers to thioacetates, demetalation took place, and the free-base porphyrin-cyclophanes **10** and **11** were isolated in moderate yields of 36 and 45%, respectively, by automated recycling GPC in chloroform. Treatment of these compounds in a CH_2Cl_2/CH_3OH solution with excess $Zn(OAc)_2$ showed slow but clean conversion of free base cyclophanes **10** and **11** to zinc complexes **1** and **2** in excellent yields of 96 and 89% after 1 day, respectively.

Having these four thioacetate functionalized cofacial porphyrin cyclophanes (**1**, **2**, **10**, and **11**) suitable for gold electrode contacting in hands, we desired to test the suitability of **1** toward single-molecule conductance experiments, as discussed in the following section.

Single-Molecule Conductance Measurements. The herein reported porphyrin cyclophane **1** was designed to absorb distance variations of an electrode pair in a molecular junction by altering the arrangement of both cofacial porphyrin subunits. The dimension of the structure and even more its division into two spatially separated porphyrin subunits raised concerns with respect to its suitability for single-molecule junctions. To investigate single-molecule junctions comprising the cofacial porphyrin cyclophane **1**, the compound was integrated in an electronic circuit using a MCBJ setup.[32−34] The MCBJ technique is particularly appealing to investigate the mechanical properties and stability of single-molecule junctions since the

https://dx.doi.org/10.1021/acs.joc.0c01957
J. Org. Chem. 2020, 85, 15072−15081

electrode displacement can be precisely controlled with high mechano-stability by a piezoelectric element, which is used to break the gold nanoelectrodes and control the distance between them after breaking. The measurements were performed in dark, ambient conditions using both fast- and self-breaking methods.[35] In the fast-breaking mode, the resistance between the electrodes is recorded while the junction is repeatedly opened and closed in a time frame of about 1 s. This allows to statistically measure the conductivity of many molecular junction configurations as a function of the distance between the electrodes. In the self-breaking mode, the junction is opened until the conductance reaches a few G_0, where the sharp electrodes are still bridged by a few gold atoms. Here, G_0 is the quantum of conductance that is defined as e^2/h with e being the elementary charge and h being the planck's constant. The distance between the electrodes is fixed, and the gold atoms reassemble into an energetically favoured conformation where upon the wire breaks. The resistance between the electrodes is measured as a function of time where the molecule typically adapts into the most stable junction configuration. More detailed information about both methods can be found in the Supporting Information.

In the fast-breaking mode, 5′113 consecutive conductance breaking traces were collected and plotted against the electrode displacement in a two-dimensional density plot (Figure 6a) of the conductance versus electrode displacement. To separate the traces showing a molecular signal from traces belonging to direct tunnelling between the electrodes, we used our unsupervised clustering algorithm[36] to split the data into two classes. The majority of traces (96%) representing the second class display an exponential decay of conductance as a function of displacement (Figure 6b), which is the characteristic of a gold−gold tunnelling junction without a bridging molecule. The first class, however, contains 4% of the total number of traces and shows conductance plateaus characteristic for a gold-molecule-gold junction. The sum of these molecular conductance traces is displayed in the two-dimensional plot of Figure 6c as a horizontal cloudlike cluster reaching out to an electrode spacing of about 2.5 nm around conductance values in the range of 10^{-5} to 10^{-6} G_0. During this stretching process, some individual conductance traces display periodic conductance variations of about 1 order of magnitude. The recorded continuous plateaus of 2.5 nm length with conductance variations in the individual traces not only corroborate the formation of a single-molecule junction but also match the expectations for the immobilized porphyrin cyclophane **1**.

By design, the structure should be able to mechanically compensate the electrode distance up to the observed breaking threshold. The spatial rearrangements of the molecular subunits during this stretching process are expected to be reflected in the transport conductance.

To corroborate the single-molecule nature of the junction and to further study its stability, 1′615 self-breaking traces were collected from the same sample. The method avoids active manipulation of the electrode spacing during the measurement but rather "fishes" for molecular structures bridging both electrodes during the spontaneous reassembling of the strained gold atoms forming the breaking point. Empty traces with lifetimes less than 20 s were filtered out because they most likely do not present the response of a molecular junction. In contrast, for most of the molecular junctions, an extended self-breaking time up to 120 s was observed, demonstrating the high stability of the gold-molecule-gold junction under ambient conditions.

To verify that in both fast- and self-breaking experiments, comparable molecules were trapped inside the gap between both electrodes, one-dimensional (1D) conductance histograms of the molecular junctions for both methods were constructed; they are displayed in Figure 7. The 1D histogram of the 4%

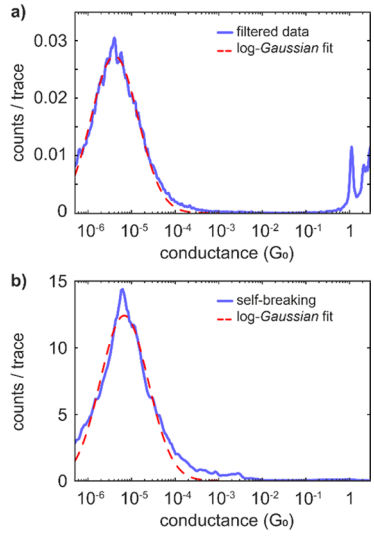

Figure 7. conductance histograms of the (a) fast-breaking and (b) self-breaking experiments. (a) The electric-blue solid line represents the filtered conductance data extracted from Figure 6c, and the red dotted line is a log-normal fit to the filtered data with a peak at 4.1×10^{-6} G_0. (b) The electric-blue solid line represents the conductance data extracted from the molecular junctions of the self-breaking experiment, and the red dotted line is a log-normal fit to the conductance data with a peak value at 8.9×10^{-6} G_0.

molecular junctions spotted in the fast-breaking experiment (Figure 7a) reveals a conductance peak with a maximum located at 4.1×10^{-6} G_0 and a spread of about 2 orders of magnitude in conductance. With the self-breaking technique, the 1D histogram features a single conductance peak, representing the most relaxed molecular junction configuration with its maximum at 6.8×10^{-6} G_0 (Figure 7b). The good agreement between both 1D histograms corroborates the reliable and repetitive formation of comparable single-molecule junctions with the here reported porphyrin cyclophane **1**. This result and the evolution of the conductance with length in the two-dimensional histograms support the intended arrangement of the molecule being immobilized by each thiol anchor group to one of both opposed electrodes of the MCBJ.

The here reported MCBJ experiments with porphyrin cyclophane **1** not only demonstrate the suitability of this mechanically adaptive molecular structure for electronic transport experiments but also already display individual molecular traces with conductance oscillations pointing at the mechano-sensitivity of the structure. However, the in-depth analysis of the electro-mechanical behavior requires not only extensive additional transport experiments and their analyses but also theoretical support, simulating how the molecules respond to mechanical stress and investigating the corresponding impact on the electronic transparency of the junction. Our current activities are geared in this direction.

■ CONCLUSIONS

Based on the experience of our previous reports, we designed the rigidly interlocked cofacial porphyrin cyclophane **1** bearing one

https://dx.doi.org/10.1021/acs.joc.0c01957
J. Org. Chem. 2020, 85, 15072−15081

thioacetate group per porphyrin subunit to anchor noble metal surfaces. Both the desired 5, pseudo 15, and the geminal thio-functionalized derivatives of the macrocycle, protected with *tert*-butyl groups, were synthesized and characterized by NMR and UV−vis spectroscopies, MS, and X-ray analysis. Last-step *trans*-protection to the thioacetates enabled covalent S−Au bond formation in our MCBJ setup. Single-molecule electronic transport experiments of the target compound **1** revealed well behaving and suitably stable single-molecule junctions of this multilevel porphyrin architecture. Specifically, the fast-breaking experiments indicated well-defined conductance features in the range from 10^{-5} to 10^{-6} G_0 with some traces showing conductance oscillations of up to an order of magnitude while stretching the junctions. On the other hand, the self-breaking measurements show the high stability of the molecular junctions. These results make the herein described new class of compounds particularly attractive for single-molecule charge transport and mechano-response studies, which are subjects of future investigations.

EXPERIMENTAL PART

General Remarks. *Reagents and Solvents.* All commercially available compounds were purchased from Sigma-Aldrich, Acros, Apollo Scientific, Alfa Aesar, and Fluorochem and used without further purification. Column chromatography was performed on silica gel P60 (40−63 μm) from SilicycleTM, and the solvents were of technical grade. TLC was performed with silica gel 60 F254 glass plates purchased from Merck.

Analytics and Instruments. NMR experiments were performed on Bruker Avance III NMR spectrometers operating at 250, 400, or 500 MHz proton frequencies. The instruments were equipped with a direct-observe 5 mm BBFO smart probe (250, 400 MHz) or an indirect-detection 5 mm BBI probe (500 MHz). All probes were equipped with actively shielded z-gradients (10 A). The chemical shifts are reported in ppm relative to tetramethylsilane or referenced to residual solvent peak, and the J values are given in Hz (±0.1 Hz). Standard Bruker pulse sequences were used, and the data was processed on Topspin 3.2 (Bruker) using twofold zero-filling in the indirect dimension. High-resolution mass spectra (HRMS) were measured on a maX-isTM4G instrument from Bruker. UV−vis absorption spectra were recorded at 20 °C on a Jasco V-770 spectrophotometer. Automated recycling GPC was performed on a Shimadzu Prominence System equipped with SDV preparative columns from Polymer Standards Service (two Showdex columns in series, 20 × 600 mm each, exclusion limit: 30,000 g/mol) with chloroform as the solvent. Single-crystal X-ray diffraction data were collected on a STOE STADIVARI diffractometer with monochromated Ga Kα (1.34143 Å) radiation at low temperature. Using Olex2, the structures were solved with the ShelXT structure solution program using Intrinsic Phasing and refined with the ShelXL refinement package using least-squares minimization. Refinement was performed with anisotropic temperature factors for all non-hydrogen atoms (disordered atoms were refined isotropically); hydrogen atoms were calculated on idealized positions.

5,15-Bis((tri-iso-propylsilyl)ethynyl)porphyrin[29] ***(6)***. A solution of 3-(tri-*iso*-propylsilyl)propiolaldehyde (4.14 mL, 16.8 mmol, 1.0 equiv) and di(1*H*-pyrrol-2-yl)methane (2.46 g, 16.8 mmol, 1.0 equiv) in CH_2Cl_2 (1.0 L) was purged with argon for 20 min at rt. Borontrifluoride-ethyl etherate (0.68 mL, 5.54 mmol, 0.3 equiv) was added, and the reaction mixture was stirred for 45 min at rt. 2,3-Dichloro-5,6-dicyano-1,4-benzoquinone (5.72 g, 25.2 mmol, 1.5 equiv) was added, and the mixture was stirred for 1 h at rt. The reaction mixture was filtered over a plug of silica eluted with CH_2Cl_2 and was concentrated under reduced pressure. Reprecipitation from CH_2Cl_2/CH_3OH gave the title compound **6** (1.56 g, 2.33 mmol, 28%) as a microcrystalline purple solid. mp >300 °C; ^{1}H NMR (500 MHz, $CDCl_3$, 298 K, δ/ppm): 10.11 (s, 2H, H_{meso}), 9.71 (d, $^3J_{HH}$ = 4.5 Hz, 4H, H_β), 9.29 (d, $^3J_{HH}$ = 4.5 Hz, 4H, H_β), 1.50−1.46 (m, 42H, H_{TIPS}), −2.71 (s, 2H, H_{NH}). ^{13}C{^{1}H} NMR (126 MHz, THF-d_8, 298 K, δ/ppm): 133.3, 130.9, 109.4, 108.1, 100.5, 99.9, 19.7, 13.0. Not all carbon atoms are visible due to π-stacking and the quadrupolar momentum of the nitrogen atoms. HRMS (ESI, +): *m/z* calcd for $C_{42}H_{55}N_4Si_2$ [M + H]$^+$, 671.3960; found, 671.3947. UV/VIS (CH_2Cl_2): λ_{max} [nm] = 416, 492, 524, 564, 600, 656.

10-Bromo-5,15-bis((tri-iso-propylsilyl)ethynyl)porphyrin ***(7)***. MgI_2 (601 mg, 2.16 mmol, 2.0 equiv) was added to a degassed solution of **6** (752 mg, 1.08 mmol, 1.0 equiv) in CH_2Cl_2/*i*Pr_2NEt (250 mL, 100:1), and the resulting mixture was stirred at rt for 1 h while the purple solution turned dark green. The solution was washed with water three times, and the combined aqueous phase was extracted with CH_2Cl_2 twice. The combined organic phase was dried over anhydrous Na_2SO_4 and concentrated under reduced pressure. The crude product was redissolved in $CHCl_3$ (0.5 L) and pyridine (5.0 mL). NBS (221 mg, 1.19 mmol, 1.1 equiv) was added, and the reaction mixture was stirred for 16 h at rt in the absence of light. The solution was washed with water three times, and the combined aqueous phase was extracted with CH_2Cl_2 twice. The combined organic phase was dried over anhydrous Na_2SO_4, concentrated under reduced pressure, and redissolved in CH_2Cl_2 (200 mL). TFA (0.40 mL, 5.40 mmol, 50 equiv) was added, and the resulting mixture was stirred at rt for 2 h while the green solution turned dark purple. The solution was washed with water three times, and the combined aqueous phase was extracted with CH_2Cl_2 twice. The combined organic phase was dried over anhydrous Na_2SO_4 and concentrated under reduced pressure. The crude product, adsorbed on silica, was subjected to column chromatography (SiO_2, toluene 1:4 cyclohexane). The desired product **7** was isolated as the second eluting purple band (352 mg, 469 mmol, 44%) as a dark blue microcrystalline solid. Substrate **6** was reisolated as the first eluting purple band (237 mg, 353 μmol, 33%). The last eluting band was found to be the over-brominated product 5,15-dibromo-10,20-bis((tri-*iso*-propylsilyl)ethynyl)porphyrin (34.0 mg, 41.0 μmol, 3.8%). mp >300 °C; ^{1}H NMR (500 MHz, THF-d_8, 298 K, δ/ppm): 10.04 (s, 1H, H_{meso}), 9.64−9.61 (m, 4H, H_β), 9.60 (d, $^3J_{HH}$ = 4.5 Hz, 2H, H_β), 9.26 (d, $^3J_{HH}$ = 4.6 Hz, 2H, H_β), 1.61−1.50 (m, 42H, H_{TIPS}), −3.05 (s, 2H, H_{NH}). ^{13}C{^{1}H} NMR (126 MHz, THF-d_8, 298 K, δ/ppm): 109.2, 108.3, 106.0, 101.7, 100.7, 19.7, 13.0. Not all carbon atoms are visible due to π-stacking and the quadrupolar momentum of the nitrogen atoms. HRMS (ESI, +): *m/z* calcd for $C_{42}H_{54}BrN_4Si_2$ [M + H]$^+$, 749.3065; found, 749.3060. UV/VIS (CH_2Cl_2): λ_{max} [nm] = 425, 499, 532, 575, 612, 673.

[10-Bromo-5,15-bis((tri-iso-propylsilyl)ethynyl)porphyrinato]-zinc(II) ***(5)***. A solution of **7** (352 mg, 469 μmol, 1.0 equiv) and $Zn(OAc)_2$ (430 mg, 2.34 mmol, 5.0 equiv) in CH_2Cl_2/CH_3OH (150 mL, 5:1) was stirred for 2 h at rt. The mixture was diluted with CH_2Cl_2 and successively washed with water. The organic phase was dried over anhydrous Na_2SO_4, filtered over a plug of silica eluted with CH_2Cl_2, and concentrated under reduced pressure yielding the title compound **5** (381 mg, 469 μmol, 100%) as a microcrystalline purple solid. mp >300 °C; ^{1}H NMR (400 MHz, THF-d_8, 298 K, δ/ppm): 10.12 (s, 1H, H_{meso}), 9.77 (d, $^3J_{HH}$ = 4.6 Hz, 2H, H_β), 9.74 (d, $^3J_{HH}$ = 4.4 Hz, 2H, H_β), 9.71 (d, $^3J_{HH}$ = 4.5 Hz, 2H, H_β), 9.32 (d, $^3J_{HH}$ = 4.4 Hz, 2H, H_β), 1.58−1.46 (m, 42H, H_{TIPS}). ^{13}C{^{1}H} NMR (126 MHz, THF-d_8, 298 K, δ/ppm): 152.6, 152.4, 150.6, 149.0, 132.9, 132.6, 131.5, 131.5, 109.8, 107.9 106.0, 100.7, 97.4, 18.6, 11.9. HRMS (ESI, −): *m/z* calcd for $C_{44}H_{54}BrN_4O_2Si_2Zn$ [M + CH_3CO_2]$^-$, 869.2266; found, 869.2269. UV/VIS (CH_2Cl_2): λ_{max} [nm] = 430, 526, 569, 613.

[10-((4-(tert-Butylthio)phenyl)ethynyl)-5,15-bis((tri-iso-propylsilyl)ethynyl) porphyrinato]zinc(II) ***(3)***. A solution of **5** (224 mg, 275 μmol, 1.0 equiv) and CuI (3.14 mg, 16.5 μmol, 0.06 equiv) in THF (30 mL) and NEt_3 (10 mL) was degassed by purging with argon for 10 min. $Pd(PPh_3)_4$ (15.9 mg, 13.8 μmol, 0.05 equiv) was added, and the resulting mixture was further degassed for 10 min. A degassed solution of *tert*-butyl(4-ethynylphenyl)sulfane (105 mg, 550 μmol, 2.0 equiv) was added *via* a syringe, and the resulting mixture was placed in a preheated oil bath at 50 °C and stirred for 16 h at this temperature. The mixture was concentrated under reduced pressure, and the residue was redissolved in a minimum amount of CH_2Cl_2, filtered over a plug of silica eluted with CH_2Cl_2, and concentrated under reduced pressure.

https://dx.doi.org/10.1021/acs.joc.0c01957
J. Org. Chem. 2020, 85, 15072−15081

The residue was reprecipitated from CH_2Cl_2/CH_3OH yielding **3** (211 mg, 229 μmol, 83%) as a microcrystalline purple solid. mp >300 °C; ^{1}H NMR (500 MHz, THF-d_8, 298 K, δ/ppm): 10.12 (s, 1H, H_{meso}), 9.83 (d, $^3J_{HH}$ = 4.5 Hz, 2H, H_β), 9.79 (d, $^3J_{HH}$ = 4.5 Hz, 2H, H_β), 9.73 (d, $^3J_{HH}$ = 4.3 Hz, 2H, H_β), 9.31 (d, $^3J_{HH}$ = 4.4 Hz, 2H, H_β), 8.14−8.07 (m, 2H, H_{Ph}), 7.81−7.75 (m, 2H, H_{Ph}), 1.58−1.49 (m, 42H, H_{TIPS}), 1.40 (s, 9H, H_{StBu}). ^{13}C{^{1}H} NMR (126 MHz, THF-d_8, 298 K, δ/ppm): 153.6, 153.0, 152.8, 151.0, 138.7, 134.9, 133.6, 132.5, 132.5, 132.2, 132.2, 125.8, 111.0, 110.1, 102.3, 102.2, 98.5, 96.8, 95.2, 47.0, 31.6, 19.7, 13.1. HRMS (ESI, −): *m/z* calcd for $C_{56}H_{67}N_4O_2SSi_2Zn$ [M + CH_3CO_2]$^-$, 979.3820; found, 979.3833. UV/VIS (CH_2Cl_2): λ_{max} [nm] (ε [M^{-1}·cm^{-1}])) = 447 (4.11 × 10^5), 581 (2.83 × 10^4), 627 (2.05 × 10^4).

2,7-Di-tert-butyl-4,5-diiodo-9,9-dimethyl-9H-xanthene[27] *(4).* A *tert*-butyllithium solution (1.7 m in pentane, 7.62 mL, 4.1 equiv) was added dropwise to a suspension of 4,5-dibromo-2,7-di-*tert*-butyl-9,9-dimethyl-9*H*-xanthene (1.52 g, 3.16 mmol, 1.0 equiv) in dry and degassed Et_2O (40 mL) at −78 °C, and the resulting mixture was stirred for 20 min at this temperature. The reaction mixture was allowed to reach rt and was stirred for 1 h. Iodine (1.76 g, 6.95 mmol, 2.2 equiv) was added at 78 °C, and the resulting mixture was stirred for 20 min at this temperature. The reaction mixture was allowed to reach rt and was stirred for 1 h. An aq. HCl solution (2 M, 10 mL) was added, and the aqueous phase was separated. The organic phase was diluted with toluene and was washed with saturated aqueous $Na_2S_2O_3$ solution, dried over anhydrous Na_2SO_4, and concentrated under reduced pressure. The crude product was recrystallized from *n*-heptane yielding **4** (1.51 g, 2.63 mmol, 83%) as an off-white solid. ^{1}H NMR (250 MHz, $CDCl_3$, 298 K, δ/ppm): 7.70 (d, $^4J_{HH}$ = 2.2 Hz, 2H, H_{Ar}), 7.36 (d, $^4J_{HH}$ = 2.2 Hz, 2H, H_{Ar}), 1.61 (s, 6H, H_{Me}), 1.31 (s, 18H, H_{tBu}). ^{13}C{^{1}H} NMR (126 MHz, $CDCl_3$, 298 K, δ/ppm): 148.3, 148.1, 134.9, 130.7, 122.9, 84.3, 35.8, 34.6, 32.1, 31.6. HRMS (ESI, +): *m/z* calcd for $C_{23}H_{28}I_2NaO$ [M + Na]$^+$, 597.0122; found, 597.0118.

8 & 9: **3** (358 mg, 388 μmol, 1.0 equiv) and **4** (223 mg, 388 μmol, 1.0 equiv) were dissolved in wet THF (30 mL), and the mixture was degassed by purging with argon for 30 min. Tetrabutylammonium fluoride (1 M, 2.3 mL, 2.33 mmol, 6.0 equiv) was added, and the resulting mixture was stirred for 1 h at rt. THF (250 mL) and NEt_3 (100 mL) were degassed by purging with argon for 1 h simultaneously. CuI (8.87 mg, 46.6 μmol, 0.12 equiv) and $Pd(PPh_3)_4$ (44.8 mg, 38.8 μmol, 0.1 equiv) were added, and the resulting mixture was further degassed by purging with argon for 10 min. The mixtures were combined via a cannula, and the resulting reaction was sealed under argon and placed into a preheated oil bath at 80 °C for 16 h with vigorous stirring. The mixture was concentrated under reduced pressure, and the residue was subjected to column chromatography (SiO_2, CH_2Cl_2 1:1 cyclohexane). The eluted mixture of **9**, **8**, and oligomeric sideproducts was concentrated and subjected to automated GPC. **9** (15 mg, 8.07 μmol) was isolated as an amorphous solid, being the slowest eluting band in 4.2% yield, and the desired 5, pseudo-15 product **8** (19.5 mg, 10.5 μmol) was isolated as an amorphous solid in 5.4% yield as the second slowest running fraction. Analytical Data for **9**. ^{1}H NMR (500 MHz, THF-d_8, 298 K, δ/ppm): 9.51 (d, $^3J_{HH}$ = 4.3 Hz, 4H, H_β), 9.46 (d, $^3J_{HH}$ = 4.2 Hz, 4H, H_β), 8.70 (d, $^3J_{HH}$ = 4.3 Hz, 4H, H_β), 8.09 (d, $^3J_{HH}$ = 4.2 Hz, 4H, H_β), 8.08 (s, 2H, H_{meso}), 8.04 (d, $^4J_{HH}$ = 2.3 Hz, 4H, H_{Xant}), 7.94−7.88 (m, 4H, H_{Ph}), 7.84 (d, $^4J_{HH}$ = 2.3 Hz, 4H, H_{Xant}), 7.77−7.71 (m, 4H, H_{Ph}), 2.03 (s, 12H, H_{Me}), 1.58 (s, 36H, H_{tBu}), 1.42 (s, 18H, H_{StBu}). ^{13}C{^{1}H} NMR (126 MHz, THF-d_8, 298 K, δ/ppm): 152.0, 151.5, 150.9, 150.5, 148.4, 147.0, 138.6, 134.0, 132.6, 131.6, 131.4, 131.3, 131.2, 130.4, 129.7, 126.2, 124.7, 113.8, 107.1, 102.2, 100.1, 98.0, 95.6, 95.0, 92.5, 46.9, 36.2, 35.6, 33.4, 33.3, 32.1, 31.8, 25.8. HRMS (ESI, −): *m/z* calcd for $C_{120}H_{103}N_8O_4S_2Zn_2$ [M + CH_3CO_2]$^-$, 1911.6132; found, 1911.6107. UV/VIS (CH_2Cl_2): λ_{max} [nm] (ε [M^{-1}·cm^{-1}]) = 437 (4.14 × 10^5), 593 (1.57 × 10^4), 642 (3.77 × 10^4). Analytical data for **8**: ^{1}H NMR (500 MHz, THF-d_8, 298 K, δ/ppm): 9.53 (d, $^3J_{HH}$ = 4.2 Hz, 4H, H_β), 9.48 (d, $^3J_{HH}$ = 4.3 Hz, 4H, H_β), 8.34 (d, $^3J_{HH}$ = 4.3 Hz, 4H, H_β), 8.20 (d, $^3J_{HH}$ = 4.2 Hz, 4H, H_β), 8.12 (s, 2H, H_{meso}), 8.07 (d, $^4J_{HH}$ = 2.3 Hz, 4H, H_{Xant}), 7.99−7.96 (m, 4H, H_{Ph}), 7.95−7.91 (m, 4H, H_{Ph}), 7.84 (d, $^4J_{HH}$ = 2.3 Hz, 4H, H_{Xant}), 2.03 (s, 12H, H_{Me}), 1.58 (s, 36H, H_{tBu}), 1.54 (s, 18H, H_{StBu}). ^{13}C{^{1}H} NMR (126 MHz, THF-d_8, 298 K, δ/ppm): 152.3, 151.5, 150.4, 150.2, 149.1, 147.0, 138.7, 134.2, 132.6, 131.9, 131.7, 131.3, 131.2, 129.9, 129.8, 126.5, 124.8, 113.8, 108.0, 102.5, 99.2, 97.9, 94.9, 94.8, 92.6, 55.0, 47.0, 36.2, 35.6, 33.4, 32.1, 31.8. HRMS (ESI, −): *m/z* calcd for $C_{120}H_{103}N_8O_4S_2Zn_2$ [M + CH_3CO_2]$^-$, 1911.6132; found, 1911.6138. UV/VIS (CH_2Cl_2): λ_{max} [nm] (ε [M^{-1}·cm^{-1}]) = 442 (3.19 × 10^5), 595 (1.26 × 10^4), 645 (3.29 × 10^4).

10: To a solution of **8** (18 mg, 9.69 μmol, 1.0 equiv) and acetyl chloride (0.12 mL, 1.70 mmol, 175 equiv) in dry and degassed toluene (4.0 mL) and acetonitrile (4.0 mL) was added bismuth(III)-trifluoromethanesulfonate (19.1 mg, 29.1 μmol, 3.0 equiv). The reaction mixture was stirred at rt for 16 h when TLC monitoring showed completion [SiO_2, CH_2Cl_2/cyclohexane (2:1)]. The mixture was poured into water and extracted with toluene. The combined organic phase was dried over anhydrous Na_2SO_4. The crude was concentrated, redissolved in $CHCl_3$, and subjected to automated GPC, yielding **10** (6.2 mg, 3.58 μmol) as an amorphous solid in 37% yield. ^{1}H NMR (500 MHz, THF-d_8, 298 K, δ/ppm): 9.55 (d, $^3J_{HH}$ = 4.4 Hz, 4H, H_β), 9.33 (d, $^3J_{HH}$ = 4.5 Hz, 4H, H_β), 9.11 (s, 2H, H_{meso}), 8.85 (d, $^3J_{HH}$ = 4.4 Hz, 4H, H_β), 8.33 (d, $^3J_{HH}$ = 4.5 Hz, 4H, H_β), 8.11−8.08 (m, 4H, H_{Ph}), 8.06 (d, $^4J_{HH}$ = 2.3 Hz, 4H, H_{Xant}), 7.87 (d, $^4J_{HH}$ = 2.3 Hz, 4H, H_{Xant}), 7.86−7.84 (m, 4H, H_{Ph}), 2.59 (s, 6H, H_{SAc}), 2.03 (s, 12H, H_{Me}), 1.58 (s, 36H, H_{tBu}), −5.22 (s, 4H, H_{NH}). ^{13}C{^{1}H} NMR (126 MHz, THF-d_8, 298 K, δ/ppm): 192.9, 150.7, 147.2, 135.8, 133.3, 131.2, 130.6, 130.1, 129.7, 127.9, 126.4, 126.3, 125.3, 113.2, 108.5, 104.2, 101.8, 99.1, 96.5, 96.0, 94.0, 93.7, 55.0, 36.3, 35.7, 33.3, 32.1, 30.8, 30.4. Not all carbon atoms are visible due to π-stacking and the quadrupolar momentum of the nitrogen atoms. HRMS (ESI, +): *m/z* calcd for $C_{114}H_{93}N_8O_4S_2$ [M + H]$^+$, 1701.6756; found, 1701.6728. UV/VIS (CH_2Cl_2): λ_{max} [nm] = 434, 621, 711.

1: A solution of **10** (1.98 mg, 1.16 μmol, 1.0 equiv) and $Zn(OAc)_2$ (10.6 mg, 58.1 μmol, 50 equiv) in CH_2Cl_2 (5.0 mL) and CH_3OH (5.0 mL) was stirred for 1 d at rt when TLC monitoring indicated completion [SiO_2, CH_2Cl_2/cyclohexane (2:1)]. The mixture was washed with water and extracted with CH_2Cl_2, dried over anhydrous Na_2SO_4, and concentrated under reduced pressure. One run over a size exclusion column (Bio Beads SX1 in toluene) gave the title compound **1** (2.03 mg, 1.11 μmol) as an amorphous solid in 96% yield. ^{1}H NMR (500 MHz, THF-d_8, 298 K, δ/ppm): 9.61 (d, $^3J_{HH}$ = 4.2 Hz, 4H, H_β), 9.42 (d, $^3J_{HH}$ = 4.3 Hz, 4H, H_β), 8.48 (s, 2H, H_{meso}), 8.44 (d, $^3J_{HH}$ = 4.3 Hz, 4H, H_β), 8.09 (d, $^4J_{HH}$ = 2.3 Hz, 4H, H_{Xant}), 8.01 (d, $^3J_{HH}$ = 4.3 Hz, 4H, H_β), 7.94−7.89 (m, 4H, H_{Ph}), 7.85−7.81 (m, 8H, H_{Ph} + H_{Xant}), 2.61 (s, 6H, H_{SAc}), 2.03 (s, 12H, H_{Me}), 1.59 (s, 36H, H_{tBu}). No ^{13}C{^{1}H} spectrum was recorded due to poor solubility and little amounts of the compound. HRMS (ESI, −): *m/z* calcd for $C_{116}H_{91}N_8O_6S_2Zn_2$ [M + CH_3CO_2]$^-$, 1883.5091; found, 1883.5120. UV/VIS (CH_2Cl_2): λ_{max} [nm] = 445, 605, 653.

11: To a solution of **9** (15 mg, 8.08 μmol, 1.0 equiv) and acetyl chloride (0.10 mL, 1.41 mmol, 175 equiv) in dry and degassed toluene (4.0 mL) and acetonitrile (4.0 mL) was added bismuth(III)-trifluoromethanesulfonate (15.9 mg, 24.2 μmol, 3.0 equiv). The reaction mixture was stirred at rt for 16 h when TLC monitoring showed completion [SiO_2, CH_2Cl_2/cyclohexane (2:1)]. The mixture was poured into water and extracted with toluene. The combined organic phase was dried over anhydrous Na_2SO_4. The crude was concentrated, redissolved in $CHCl_3$, and subjected to automated GPC, yielding **11** (7.5 mg, 4.44 μmol) as an amorphous solid in 55% yield. ^{1}H NMR (500 MHz, THF-d_8, 298 K, δ/ppm): 9.45 (d, $^3J_{HH}$ = 4.5 Hz, 4H, H_β), 9.37 (d, $^3J_{HH}$ = 4.4 Hz, 4H, H_β), 9.09 (d, $^3J_{HH}$ = 4.5 Hz, 4H, H_β), 8.62 (s, 2H, H_{meso}), 8.48 (d, $^3J_{HH}$ = 4.4 Hz, 4H, H_β), 8.10−8.07 (m, 4H, H_{Ph}), 8.01 (d, $^4J_{HH}$ = 2.3 Hz, 4H, H_{Xant}), 7.87 (d, $^4J_{HH}$ = 2.3 Hz, 4H, H_{Xant}), 7.67−7.63 (m, 4H, H_{Ph}), 2.54 (s, 6H, H_{SAc}), 2.05 (s, 6H, H_{Me}), 2.04 (s, 6H, H_{Me}), 1.56 (s, 36H, H_{tBu}), −5.72 (s, 4H, H_{NH}). ^{13}C{^{1}H} NMR (126 MHz, THF-d_8, 298 K, δ/ppm): 192.8, 150.9, 147.2, 135.6, 133.2, 131.2, 130.1, 129.5, 126.2, 125.2, 113.3, 107.2, 101.4, 100.3, 97.1, 96.5, 94.4, 93.8, 55.0, 36.3, 35.7, 32.1, 30.8. HRMS (ESI, +): *m/z* calcd for $C_{114}H_{92}N_8O_4S_2$ [M]$^+$, 1700.6677; found, 1700.6646. UV/VIS (CH_2Cl_2): λ_{max} [nm] = 434, 617, 707.

2: A solution of **11** (2 mg, 1.17 μmol, 1.0 equiv) and $Zn(OAc)_2$ (10.7 mg, 58.5 μmol, 50 equiv) in CH_2Cl_2 (5.0 mL) and CH_3OH (5.0 mL) was stirred for 1 d at rt when TLC monitoring indicated completion

https://dx.doi.org/10.1021/acs.joc.0c01957
J. Org. Chem. 2020, 85, 15072−15081

[SiO_2, CH_2Cl_2/cyclohexane (2:1)]. The mixture was washed with water and extracted with CH_2Cl_2, dried over anhydrous Na_2SO_4, and concentrated under reduced pressure. One run over a size exclusion column (Bio Beads SX1 in toluene) gave the title compound **2** (1.9 mg, 1.04 μmol) as an amorphous solid in 89% yield. ^{1}H NMR (500 MHz, THF-d_8, 298 K, δ/ppm): 9.52 (d, $^3J_{HH}$ = 4.3 Hz, 4H, H_β), 9.46 (d, $^3J_{HH}$ = 4.2 Hz, 4H, H_β), 8.72 (d, $^3J_{HH}$ = 4.3 Hz, 4H, H_β), 8.11 (d, $^3J_{HH}$ = 4.2 Hz, 4H, H_β), 8.10 (s, 2H, H_{meso}), 8.05 (d, $^4J_{HH}$ = 2.3 Hz, 4H, H_{Xant})), 7.94 (d, $^3J_{HH}$ = 8.1 Hz, 4H, H_{Ph}), 7.85 (d, $^4J_{HH}$ = 2.3 Hz, 4H, H_{Xant})), 7.62 (d, $^3J_{HH}$ = 8.1 Hz, 4H, H_{Ph})), 2.51 (s, 6H, H_{SAc}), 2.04 (s, 12H, H_{Me}), 1.58 (s, 36H, H_{tBu}). ^{13}C{^{1}H} NMR (126 MHz, THF-d_8, 298 K, δ/ppm): 192.9, 152.0, 151.5, 151.0, 150.5, 148.4, 147.0, 135.4, 133.0, 131.6, 131.4, 131.3, 131.2, 130.4, 129.7, 129.3, 126.7, 124.7, 113.9, 107.2, 102.2, 99.9, 98.0, 95.5, 95.2, 92.5, 36.3, 35.6, 33.4, 33.3, 32.1, 30.8. HRMS (ESI, +): *m/z* calcd for $C_{114}H_{88}N_8O_4S_2Zn_2$ $[M]^+$, 1824.4947; found, 1824.4923. UV/VIS (CH_2Cl_2): λ_{max} [nm] = 441, 601, 648.

■ ASSOCIATED CONTENT

Supporting Information

The Supporting Information is available free of charge at https://pubs.acs.org/doi/10.1021/acs.joc.0c01957.

Synthetic overview, NMR spectra, HRMS reports, UV−vis spectra, crystallographic data, and details about the MCBJ method (PDF)

Primary NMR FID files for compounds 1−11 (ZIP)

Accession Codes

CCDC 2019591−2019592 contain the supplementary crystallographic data for this paper. These data can be obtained free of charge via www.ccdc.cam.ac.uk/data_request/cif, or by emailing data_request@ccdc.cam.ac.uk, or by contacting The Cambridge Crystallographic Data Centre, 12 Union Road, Cambridge CB2 1EZ, UK; fax: +44 1223 336033.

■ AUTHOR INFORMATION

Corresponding Authors

Herre S. J. van der Zant − *Kavli Institute of Nanoscience, Delft University of Technology, 2600 GA Delft, The Netherlands;* orcid.org/0000-0002-5385-0282; Email: H.S.J.vanderZant@tudelft.nl

Marcel Mayor − *Department of Chemistry, University of Basel, 4056 Basel, Switzerland; Institute for Nanotechnology (INT), Karlsruhe Institute of Technology (KIT), 76021 Karlsruhe, Germany; Lehn Institute of Functional Materials (LIFM), School of Chemistry, Sun Yat-Sen University (SYSU), 510275 Guangzhou, China;* orcid.org/0000-0002-8094-7813; Email: marcel.mayor@unibas.ch

Authors

Patrick Zwick − *Department of Chemistry, University of Basel, 4056 Basel, Switzerland;* orcid.org/0000-0003-2053-1768

Chunwei Hsu − *Kavli Institute of Nanoscience, Delft University of Technology, 2600 GA Delft, The Netherlands*

Maria El Abbassi − *Kavli Institute of Nanoscience, Delft University of Technology, 2600 GA Delft, The Netherlands;* orcid.org/0000-0001-5177-6528

Olaf Fuhr − *Institute for Nanotechnology (INT) and Karlsruhe Nano Micro Facility (KNMF), Karlsruhe Institute of Technology (KIT), 76021 Karlsruhe, Germany*

Dieter Fenske − *Institute for Nanotechnology (INT) and Karlsruhe Nano Micro Facility (KNMF), Karlsruhe Institute of Technology (KIT), 76021 Karlsruhe, Germany*

Diana Dulić − *Department of Physics and Department of Electrical Engineering, Faculty of Physical and Mathematical Sciences, University of Chile, 8330015 Santiago, Chile;* orcid.org/0000-0002-8302-5507

Complete contact information is available at: https://pubs.acs.org/10.1021/acs.joc.0c01957

Author Contributions

[¶]P.Z. and C.H. contributed equally to this work.

Notes

The authors declare no competing financial interest.

■ ACKNOWLEDGMENTS

This study was supported by the EU through a RISE(DAFNEOX) project, SEP 210165479, and partially funded by the FET open project QuIET (no. 767187). The device fabrication was done at the Kavli Nanolab at Delft. Generous financial support by the Swiss National Science Foundation (SNF grant number 200020-178808) is gratefully acknowledged. D.D. acknowledges support by the Fondecyt Regular Project 1181080, and M.M. acknowledges support by the 111 project (90002-18011002).

■ REFERENCES

(1) Guo, C.; Wang, K.; Zerah-Harush, E.; Hamill, J.; Wang, B.; Dubi, Y.; Xu, B. Molecular rectifier composed of DNA with high rectification ratio enabled by intercalation. *Nat. Chem.* **2016**, *8*, 484−490.

(2) Valdiviezo, J.; Palma, J. L. Molecular Rectification Enhancement Based On Conformational and Chemical Modifications. *J. Phys. Chem. C* **2018**, *122*, 2053−2063.

(3) Zhao, J.; Yu, C.; Wang, N.; Liu, H. Molecular Rectification Based on Asymmetrical Molecule−Electrode Contact. *J. Phys. Chem. C* **2010**, *114*, 4135−4141.

(4) Bi, H.; Palma, C.-A.; Gong, Y.; Hasch, P.; Elbing, M.; Mayor, M.; Reichert, J.; Barth, J. V. Voltage-Driven Conformational Switching with Distinct Raman Signature in a Single-Molecule Junction. *J. Am. Chem. Soc.* **2018**, *140*, 4835−4840.

(5) Gerhard, L.; Edelmann, K.; Homberg, J.; Valášek, M.; Bahoosh, S. G.; Lukas, M.; Pauly, F.; Mayor, M.; und Wulfhekel, W. An electrically actuated molecular toggle switch. *Nat. Commun.* **2017**, *8*, 14672.

(6) Kim, Y.; Hellmuth, T. J.; Sysoiev, D.; Pauly, F.; Pietsch, T.; Wolf, J.; Erbe, A.; Huhn, T.; Groth, U.; Steiner, U. E.; Scheer, E. Charge Transport Characteristics of Diarylethene Photoswitching Single-Molecule Junctions. *Nano Lett.* **2012**, *12*, 3736−3742.

(7) Pleux, L. L.; Kapatsina, E.; Hildesheim, J.; Häussinger, D.; und Mayor, M. A Molecular Turnstile as an E-Field-Triggered Single-Molecule Switch: Concept and Synthesis. *Eur. J. Org Chem.* **2017**, 3165−3178.

(8) Schwarz, F.; Kastlunger, G.; Lissel, F.; Egler-Lucas, C.; Semenov, S. N.; Venkatesan, K.; Berke, H.; Stadler, R.; Lörtscher, E. Field-induced conductance switching by charge-state alternation in organometallic single-molecule junctions. *Nat. Nanotechnol.* **2016**, *11*, 170−176.

(9) Wirth, J.; Hatter, N.; Drost, R.; Umbach, T. R.; Barja, S.; Zastrow, M.; Rück-Braun, K.; Pascual, J. I.; Saalfrank, P.; Franke, K. J. Diarylethene Molecules on a Ag(111) Surface: Stability and Electron-Induced Switching. *J. Phys. Chem. C* **2015**, *119*, 4874−4883.

(10) Kolivoska, V.; Moreno-García, P.; Kaliginedi, V.; Hong, W.; Mayor, M.; Weibel, N.; Wandlowski, T. Electron transport through catechol-functionalized molecular rods. *Electrochim. Acta* **2013**, *110*, 709−717.

(11) Frisenda, R.; Janssen, V. A. E. C.; Grozema, F. C.; van der Zant, H. S. J.; Renaud, N. Mechanically controlled quantum interference in individual π -stacked dimers. *Nat. Chem.* **2016**, *8*, 1099−1104.

(12) Fu, T.; Smith, S.; Camarasa-Gómez, M.; Yu, X.; Xue, J.; Nuckolls, C.; Evers, F.; Venkataraman, L.; Wei, S. Enhanced coupling through π-

stacking in imidazole-based molecular junctions. *Chem. Sci.* **2019**, *10*, 9998−10002.
(13) Brandl, T.; El Abbassi, M.; Stefani, D.; Frisenda, R.; Harzmann, G. D.; van der Zant, H. S. J.; Mayor, M. Enhanced Separation Concept (ESC): Removing the Functional Subunit from the Electrode by Molecular Design. *Eur. J. Org Chem.* **2019**, 5334−5343.
(14) Frisenda, R.; Harzmann, G. D.; Celis Gil, J. A.; Thijssen, J. M.; Mayor, M.; van der Zant, H. S. J. Stretching-Induced Conductance Increase in a Spin-Crossover Molecule. *Nano Lett.* **2016**, *16*, 4733−4737.
(15) Nejedlý, J.; Šámal, M.; Rybáček, J.; Sánchez, I. G.; Houska, V.; Warzecha, T.; Vacek, J.; Sieger, L.; Buděšínský, M.; Bednárová, L.; Fiedler, P.; Císařová, I.; Starý, I.; Stará, I. G. Synthesis of Racemic, Diastereopure, and Enantiopure Carba- or Oxa[5]-, [6]-, [7]-, and -[19]helicene (Di)thiol Derivatives. *J. Org. Chem.* **2020**, *85*, 248−276.
(16) Stefani, D.; Weiland, K. J.; Skripnik, M.; Hsu, C.; Perrin, M. L.; Mayor, M.; Pauly, F.; van der Zant, H. S. J. Large Conductance Variations in a Mechanosensitive Single-Molecule Junction. *Nano Lett.* **2018**, *18*, 5981−5988.
(17) Yang, H.; Liu, J.; Wen, X.; Lu, C. Molecular mechanism of photosystem I assembly in oxygenic organisms. *Biochim. Biophys. Acta* **2015**, *1847*, 838−848.
(18) Jurow, M.; Schuckman, A. E.; Batteas, J. D.; Drain, C. M. Porphyrins as molecular electronic components of functional devices. *Coord. Chem. Rev.* **2010**, *254*, 2297−2310.
(19) Balaban, T. S. Tailoring Porphyrins and Chlorins for Self-Assembly in Biomimetic Artificial Antenna Systems. *Acc. Chem. Res.* **2005**, *38*, 612−623.
(20) Horn, S.; Dahms, K.; Senge, M. O. Synthetic transformations of porphyrins − Advances 2004-2007. *J. Porphyrins Phthalocyanines* **2008**, *12*, 1053−1077.
(21) Leary, E.; Limburg, B.; Alanazy, A.; Sangtarash, S.; Grace, I.; Swada, K.; Esdaile, L. J.; Noori, M.; González, M. T.; Rubio-Bollinger, G.; Sadeghi, H.; Hodgson, A.; Agraït, N.; Higgins, S. J.; Lambert, C. J.; Anderson, H. L.; Nichols, R. J. Bias-Driven Conductance Increase with Length in Porphyrin Tapes. *J. Am. Chem. Soc.* **2018**, *140*, 12877−12883.
(22) Li, Z.; Smeu, M.; Ratner, M. A.; Borguet, E. Effect of Anchoring Groups on Single Molecule Charge Transport through Porphyrins. *J. Phys. Chem. C* **2013**, *117*, 14890−14898.
(23) Li, Z.; Park, T.-H.; Rawson, J.; Therien, M. J.; Borguet, E. Quasi-Ohmic Single Molecule Charge Transport through Highly Conjugated meso-to-meso Ethyne-Bridged Porphyrin Wires. *Nano Lett.* **2012**, *12*, 2722−2727.
(24) Sedghi, G.; Sawada, K.; Esdaile, L. J.; Hoffmann, M.; Anderson, H. L.; Bethell, D.; Haiss, W.; Higgins, S. J.; Nichols, R. J. Single Molecule Conductance of Porphyrin Wires with Ultralow Attenuation. *J. Am. Chem. Soc.* **2008**, *130*, 8582−8583.
(25) El Abbassi, M.; Zwick, P.; Rates, A.; Stefani, D.; Prescimone, A.; Mayor, M.; van der Zant, H. S. J.; Dulić, D. Unravelling the conductance path through single-porphyrin junctions. *Chem. Sci.* **2019**, *10*, 8299−8305.
(26) Zwick, P.; Weiland, K. J.; Malinčík, J.; Stefani, D.; Häussinger, D.; van der Zant, H. S. J.; Dulić, D.; Mayor, M. Mechanical Fixation by Porphyrin Connection: Synthesis and Transport Studies of a Bicyclic Dimer. *J. Org. Chem.* **2020**, *85*, 118−128.
(27) Morisaki, Y.; Chujo, Y. Construction of benzene ring-layered polymers. *Tetrahedron Lett.* **2005**, *46*, 2533−2537.
(28) Błaszczyk, A.; Elbing, M.; und Mayor, M. Bromine catalyzed conversion of S-tert-butyl groups into versatile and, for self-assembly processes accessible, acetyl-protected thiols. *Org. Biomol. Chem.* **2004**, *2*, 2722−2724.
(29) Screen, T. E. O.; Lawton, K. B.; Wilson, G. S.; Dolney, N.; Ispasoiu, R.; Goodson III, T.; Martin, S. J.; Bradley, D. D. C.; Anderson, H. L. Synthesis and third order nonlinear optics of a new soluble conjugated porphyrin polymer. *J. Mater. Chem.* **2001**, *11*, 312−320.
(30) Wilson, G. S.; und Anderson, H. L. A conjugated triple strand porphyrin array. *Chem. Commun.* **1999**, 1539−1540.
(31) Zanetti-Polzi, L.; Amadei, A.; Djemili, R.; Durot, S.; Schoepff, L.; Heitz, V.; Ventura, B.; und Daidone, I. Interpretation of Experimental Soret Bands of Porphyrins in Flexible Covalent Cages and in Their Related Ag(I) Fixed Complexes. *J. Phys. Chem. C* **2019**, *123*, 13094−13103.
(32) Frisenda, R.; Stefani, D.; van der Zant, H. S. J. Quantum Transport through a Single Conjugated Rigid Molecule, a Mechanical Break Junction Study. *Acc. Chem. Res.* **2018**, *51*, 1359−1367.
(33) Martin, C. A.; Smit, R. H. M.; Egmond, R.; van der Zant, H. S. J.; und van Ruitenbeek, J. M. A versatile low-temperature setup for the electrical characterization of single-molecule junctions. *Rev. Sci. Instrum.* **2011**, *82*, 053907.
(34) Frisenda, R.; Perrin, M. L.; Valkenier, H.; Hummelen, J. C.; van der Zant, H. S. J. Statistical analysis of single-molecule breaking traces. *Phys. Status Solidi B* **2013**, *250*, 2431−2436.
(35) Tsutsui, M.; Shoji, K.; Taniguchi, M.; Kawai, T. Formation and Self-Breaking Mechanism of Stable Atom-Sized Junctions. *Nano Lett.* **2008**, *8*, 345−349.
(36) Cabosart, D.; El Abbassi, M.; Stefani, D.; Frisenda, R.; Calame, M.; van der Zant, H. S. J.; Perrin, M. L. A reference-free clustering method for the analysis of molecular break-junction measurements. *Appl. Phys. Lett.* **2019**, *114*, 143102.

https://dx.doi.org/10.1021/acs.joc.0c01957
J. Org. Chem. 2020, 85, 15072−15081